Research Article | Vol. 25, No. 23 | 13 Nov 2017 | OPTICS EXPRESS 28246
Optics EXPRESS

Optical properties and resonant cavity modes in axial InGaN/GaN nanotube microcavities

P. -M. Coulon,[1,*] J. R. Pugh,[2] M. Athanasiou,[3] G. Kusch,[4] E. D. Le Boulbar,[1] A. Sarua,[2] R. Smith,[3] R. W. Martin,[4] T. Wang,[3] M. Cryan,[2] D. W. E. Allsopp,[1] and P. A. Shields[1]

[1]Department of Electronic and Electrical Engineering, University of Bath, BA2 7AY, UK
[2]Department of, University of Bristol, BS8 1UB, UK
[3]Department of Electronic and Electrical Engineering, University of Sheffield, S1 4DE, UK
[4]Department of Physics, SUPA, University of Strathclyde, G4 0NG, UK
[*]P.Coulon@bath.ac.uk

Abstract: Microcavities based on group-III nitride material offer a notable platform for the investigation of light-matter interactions as well as the development of devices such as high efficiency light emitting diodes (LEDs) and low-threshold nanolasers. Disk or tube geometries in particular are attractive for low-threshold lasing applications due to their ability to support high finesse whispering gallery modes (WGMs) and small modal volumes. In this article we present the fabrication of homogenous and dense arrays of axial InGaN/GaN nanotubes via a combination of displacement Talbot lithography (DTL) for patterning and inductively coupled plasma top-down dry-etching. Optical characterization highlights the homogeneous emission from nanotube structures. Power-dependent continuous excitation reveals a non-uniform light distribution within a single nanotube, with vertical confinement between the bottom and top facets, and radial confinement within the active region. Finite-difference time-domain simulations, taking into account the particular shape of the outer diameter, indicate that the cavity mode of a single nanotube has a mixed WGM-vertical Fabry-Perot mode (FPM) nature. Additional simulations demonstrate that the improvement of the shape symmetry and dimensions primarily influence the Q-factor of the WGMs whereas the position of the active region impacts the coupling efficiency with one or a family of vertical FPMs. These results show that regular arrays of axial InGaN/GaN nanotubes can be achieved via a low-cost, fast and large-scale process based on DTL and top-down etching. These techniques open a new perspective for cost effective fabrication of nano-LED and nano-laser structures along with bio-chemical sensing applications.

OCIS codes: (220.0220) Optical design and fabrication; (220.4241) Nanostructure fabrication; (250.0250) Optoelectronics; (250.1500) Cathodoluminescence; (250.5230) Photoluminescence; (260.0260) Physical optics; (260.5740) Resonance; (260.6970) Total internal reflection.

References and links

1. L. Rayleigh, "The problem of the whispering gallery," Philos. Mag. **20**, 1001–1004 (1910).
2. A. B. Matsko and V. S. Ilchenko, "Optical Resonators With Whispering-Gallery Modes—Part I: Basics," IEEE J. Sel. Top. Quantum Electron. **12**, 3 (2006).
3. J. M. Redwing, D. A. S. Loeber, N. G. Anderson, M. A. Tischler, and J. S. Flynn, "An optically pumped GaN–AlGaN vertical cavity surface emitting laser," Appl. Phys. Lett. **69**, 1 (1996).
4. T. C. Lu, C. C. Kao, H. C. Kuo, G. S. Huang, and S. C. Wang, "CW lasing of current injection blue GaN-based vertical cavity surface emitting laser," Appl. Phys. Lett. **92**, 141102 (2008).
5. V. S. Ilchenko and A. B. Matsko, "Optical resonators with whispering-gallery modes—Part II: Applications," IEEE J. Sel. Top. Quantum Electron. **12**, 1 (2006).
6. J. Goldberger, R. Fan, and P. Yang, "Inorganic nanotubes: a novel platform for nanofluidics," Acc. Chem. Res. **39**(4), 239–248 (2006).
7. A. M. Armani, R. P. Kulkarni, S. E. Fraser, R. C. Flagan, and K. J. Vahala, "Label-free, single-molecule detection with optical microcavities," Science **317**(5839), 783–787 (2007).

#302917 https://doi.org/10.1364/OE.25.028246
Journal © 2017 Received 31 Jul 2017; revised 18 Sep 2017; accepted 15 Oct 2017; published 31 Oct 2017

Optics EXPRESS

8. F. Vollmer and S. Arnold, "Whispering-gallery-mode biosensing: label-free detection down to single molecules," Nat. Methods **5**(7), 591–596 (2008).
9. S. Chang, N. B. Rex, R. K. Chang, G. Chong, and L. J. Guido, "Stimulated emission and lasing in whispering-gallery mods of GaN microdisck cavities," Appl. Phys. Lett. **75**, 166–168 (1999).
10. M. Athanasiou, R. Smith, B. Liu, and T. Wang, "Room temperature continuous-wave green lasing from an InGaN microdisk on silicon," Sci. Rep. **4**, 7250 (2014).
11. T. Kouno, M. Sakai, K. Kishino, and K. Hara, "Sensing operations based on hexagonal GaN microdisks acting as whispering-gallery mode optical microcavities," Opt. Lett. **40**(12), 2866–2869 (2015).
12. K. H. Li, Z. Ma, and H. W. Choi, "Single-mode whispering gallery lasing from metal-clad GaN nanopillars," Opt. Lett. **37**(3), 374–376 (2012).
13. C. Tessarek, R. Röder, T. Michalsky, S. Geburt, H. Franke, R. Schmidt-Grund, M. Heilmann, B. Hoffmann, C. Ronning, M. Grundmann, and S. Christiansen, "Improving the optical properties of self-catalyzed GaN microrods toward whispering gallery mode lasing," ACS Photonics **1**, 990–997 (2014).
14. K. H. Li, Y. F. Cheung, and H. W. Choi, "Whispering gallery mode lasing in optically isolated III-nitride nanorings," Opt. Lett. **40**(11), 2564–2567 (2015).
15. A.-L. Henneghien, B. Gayral, Y. Désières, and J.-M. Gérard, "Simulation of waveguiding and emitting properties of semiconductor nanowires with hexagonal or circular sections," J. Opt. Soc. Am. **26**(12), 2396 (2009).
16. C. P. Dietrich, M. Lange, T. Bontgen, and M. Grundmann, "The corner effect in hexagonal whispering gallery microresonators," Appl. Phys. Lett. **101**, 141116 (2012).
17. T. Kouno, K. Kishino, T. Suzuki, and M. Sakai, "Lasing Actions in GaN Tiny Hexagonal Nanoring Resonators," IEEE Photonics J. **2**, 1027 (2010).
18. P. M. Coulon, M. Hugues, B. Alloing, E. Beraudo, M. Leroux, and J. Zúñiga-Pérez, "GaN microwires as optical microcavities: Whispering gallery modes Vs Fabry-Perot modes," Opt. Express **20**(17), 18707–18716 (2012).
19. J. Sellés, C. Brimont, G. Cassabois, P. Valvin, T. Guillet, I. Roland, Y. Zeng, X. Checoury, P. Boucaud, M. Mexis, F. Semond, and B. Gayral, "Deep-UV nitride-on-silicon microdisk lasers," Sci. Rep. **6**, 21650 (2016).
20. C. Tessarek, M. Heilmann, and S. Christiansen, "Whispering gallery modes in GaN microdisks, microrods and nanorods grown by MOVPE," Phys. Status Solidi., C Curr. Top. Solid State Phys. **11**(3–4), 794–797 (2014).
21. Q. Li, J. B. Wright, W. W. Chow, T. S. Luk, I. Brener, L. F. Lester, and G. T. Wang, "Single-mode GaN nanowire lasers," Opt. Express **20**(16), 17873–17879 (2012).
22. C. Li, S. Liu, A. Hurtado, J. B. Wright, H. Xu, T. S. Luk, J. J. Figiel, I. Brener, S. R. J. Brueck, and G. T. Wang, "Annular-Shaped Emission from Gallium Nitride Nanotube Lasers," ACS Photonics **2**(8), 1025–1029 (2015).
23. C. Li, J. B. Wright, S. Liu, P. Lu, J. J. Figiel, B. Leung, W. W. Chow, I. Brener, D. D. Koleske, T. S. Luk, D. F. Feezell, S. R. J. Brueck, and G. T. Wang, "Nonpolar InGaN/GaN core–shell single nanowire lasers," Nano Lett. **17**(2), 1049–1055 (2017).
24. K. C. Zeng, L. Dai, J. Y. Lin, and H. X. Jiang, "Optical resonance modes in InGaN/GaN multiple-quantum-well microring cavities," Appl. Phys. Lett. **75**, 2563 (1999).
25. T. Kouno, K. Kishino, and A. Kikuchi, "Whispering gallery mode in periodic InGaN-based hexagonal nanoring arrays grown by rf-MBE using Ti-mask selective-area growth," Phys. Status Solidi., A Appl. Mater. Sci. **207**(1), 37–40 (2010).
26. S. Paul, K. Maier, A. Das, F. Furtmayr, A. Helwig, J. Teubert, E. Monroy, G. Müller, and M. Eickhoff, "III-nitride nanostructures for optical gas detection and pH sensing," Proc. SPIE **8725**, 87250K (2013).
27. H. Abe, M. Narimatsu, T. Watanabe, T. Furumoto, Y. Yokouchi, Y. Nishijima, S. Kita, A. Tomitaka, S. Ota, Y. Takemura, and T. Baba, "Living-cell imaging using a photonic crystal nanolaser array," Opt. Express **23**(13), 17056–17066 (2015).
28. R. Kirste, N. Rohrbaugh, I. Bryan, Z. Bryan, R. Collazo, and A. Ivanisevic, "Electronic Biosensors Based on III-Nitride Semiconductors," Annu. Rev. Anal. Chem. (Palo Alto, Calif.) **8**, 149–169 (2015).
29. J. Goldberger, R. He, Y. Zhang, S. Lee, H. Yan, H.-J. Choi, and P. Yang, "Single-crystal gallium nitride nanotubes," Nature **422**(6932), 599–602 (2003).
30. C. Hemmingsson, G. Pozina, S. Khromov, and B. Monemar, "Growth of GaN nanotubes by halide vapor phase epitaxy," Nanotechnology **22**(8), 085602 (2011).
31. Lumerical Solutions, Inc., http://www.lumerical.com/tcad-products/fdtd/
32. P. R. Edwards, L. K. Jagadamma, J. Bruckbauer, C. Liu, P. Shields, D. Allsopp, T. Wang, and R. W. Martin, "High-resolution cathodoluminescence hyperspectral imaging of nitride nanostructures," Microsc. Microanal. **18**(6), 1212–1219 (2012).
33. M. Mexis, S. Sergent, T. Guillet, C. Brimont, T. Bretagnon, B. Gil, F. Semond, M. Leroux, D. Néel, S. David, X. Chécoury, and P. Boucaud, "High quality factor nitride-based optical cavities: microdisks with embedded GaN/Al(Ga)N quantum dots," Opt. Lett. **36**(12), 2203–2205 (2011).
34. M. T. Hill and M. C. Gather, "Advances in small lasers," Nat. Photonics **8**, 908–918 (2014).
35. Y. Zhang, X. Zhang, K. H. Li, Y. F. Cheung, C. Feng, and H. W. Choi, "Advances in III-nitride semiconductor microdisk lasers," Phys. Status Solidi., A Appl. Mater. Sci. **212**, 960–973 (2015).

Optics EXPRESS

1. Introduction

III-Nitride micron and submicron cavities such as disks, rods, rings and tubes shaped structures, in which light can be confined around their periphery by total internal reflection [1,2], have been proposed as a way to overcome the difficulties of incorporating mirrors in vertical-cavity surface-emitting lasers [3,4]. The strong light confinement and high Q-factor resulting from the whispering-gallery modes (WGMs) supported in such cavities is of great interest for low-power consumption light emitting devices, photonic applications [5], photodetectors and biochemical sensors [6–8]. Several studies have been performed with various cavity geometries to achieve mode-enhanced optical lasing action in a single structure [9–14]. However, the optical modal properties (i.e. the frequency, the spacing, the Q-factor) and even the nature of the resonant modes (i.e whispering-gallery or Fabry-Perot) can be highly influenced by the geometry of the cavity (e.g. circular, hexagonal or distorted) [15–18], the dimensions (i.e. height and diameter) [17,19–22] and the integration and position of the active gain medium [14,15,23].

While microdisk cavities are typically designed with a low aspect ratio (i.e. $t < \lambda/2n$, with t the thickness of the cavity, λ the wavelength of the dipole, n the refractive index) to emphasize their WGM character, particularly for micro-laser applications, ring based cavities of subwavelength (i.e. nanoscale) dimension are predicted to have a superior optical confinement, due to the absence of higher-order radial modes [17,24]. When combined with diameters in the order of the operation wavelength, this can lead to a reduced number of WGMs contributing to lasing [14,17]. In contrast, for higher aspect ratio cavities such as rods and tubes, reflection between the top and bottom faces occurs ($t >> \lambda/2n$) and the Fabry-Perot (FP) character of the cavity modes becomes more dominant over their WG nature, especially for subwavelength diameters [18], thus leading to FP lasing [21–23]. However, by combining the superior radial optical confinement of tubular geometry with the integration of an active region, either axially or radially, higher coupling efficiency of the light with the cavity modes will occur near the rim of the tube compared to the end face [25], thus promoting WG lasing. Therefore, high-aspect-ratio axial tubular cavities fabricated from planar LED structures by top-down etching, with the active region decoupled from the underlying planar buffer layer, provide the opportunity to fabricate electrically injected nano-lasers and photonic-electronic integrated circuits, independently of the nature of the substrate, which could even be visible light absorbing silicon. The high Q-factors of WGMs also provide scope for an increased sensitivity of the tubular cavities in sensors applications, involving resonant frequency shifts, change of peak transmission or a change in Q-factor. Further, the chemical stability and bio-compatibility of III-Nitride-based optical resonant cavities provide opportunities for their integration into bio-chemical sensing devices [26–28].

A variety of techniques have been utilized to synthesize tubular nanostructures including epitaxial casting [29], vapor–liquid–solid growth [30], selective area growth [25] and top-down etching [22]. These approaches can lead not only to inhomogeneities in terms of dimensions and optical properties but also to difficulties in integrating axial active regions. To date, there are no reports of III-nitride nanotube cavities containing an axial active region. In this paper, we demonstrate the fabrication of large-scale homogenous dense arrays of axial InGaN/GaN nanotubes from a planar InGaN/GaN LED structure by a combination of Displacement Talbot lithography (DTL) and optimized inductively coupled plasma (ICP) top-down etching. The optical properties of these nanotubes along with their modal properties have been studied by cathodoluminescence (CL), micro-photoluminescence (μPL) and confocal photoluminescence (PL) and compared with Finite-Difference Time-Domain (FDTD) simulations [31]. The obtained results demonstrate the mixed WG and FP nature of the cavity modes.

Optics EXPRESS

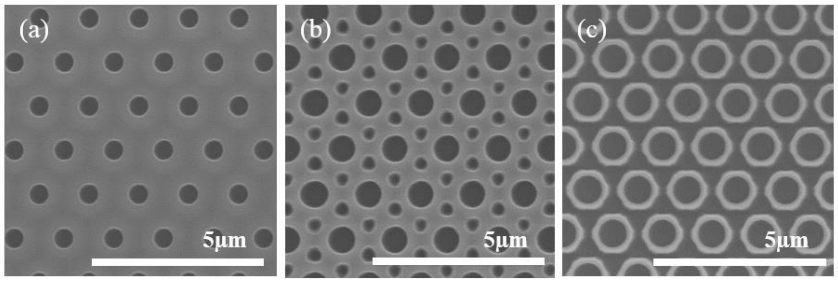

Fig. 1. SEM plan-view image of the resist mask after DTL exposure for a dose of (a) 100 mJ/cm^2, (b) 200 mJ/cm^2 and (c) 480 mJ/cm^2.

2. InGaN/GaN nanotube fabrication

The InGaN/GaN single quantum well (SQW) LED structure used for this study was grown on (0001) sapphire substrates by metal-organic vapor phase epitaxy (MOVPE) and consisted of a 5.6 µm n-type GaN:Si layer followed by a 2-3 nm InGaN SQW and a p-type GaN:Mg capping layer of 600 nm. DTL (EULITHA PhableR 100) was used to pattern a hard etch mask consisting in an array of nanorings. Firstly, a 600 nm SiN_x layer was deposited by PECVD onto the full 50 mm diameter LED wafer. Secondly, a 190 nm layer of bottom antireflective coating (BARC) and 600 nm of high contrast positive resist were spun onto the SiN_x. Then, the structure was exposed with the DTL system through an optical mask consisting of 800 nm diameter holes in a hexagonal arrangement with a 1.5 µm pitch. Further details of the overall DTL exposure and resist development parameters can be found in the Experimental details section. High-aspect-ratio nanorings of resist were obtained by carefully optimizing the exposure dose, as depicted in Fig. 1. For a low exposure dose of 100 mJ/cm^2, a pattern of holes with an opening diameter of ~500 nm are transferred into the resist [Fig. 1(a)]. Increasing the exposure dose to 200 mJ/cm^2 leads to larger hole openings of diameter ~700 nm along with the formation of a secondary pattern [Fig. 1(b)]. This pattern surrounds the first primary hole pattern and is composed of six hexagonal triangular-like holes with a smaller opening diameter. Further increasing the exposure dose to 480 mJ/cm^2, the diameter of the hexagonal triangular-like dots becomes larger and finally merge to create a nanoring pattern having an inner diameter of ~850 nm and a wall width of ~100-150 nm [Fig. 1(c)]. The non-circularity of the outer diameter, with a hexagonal like shape, is intrinsic to the fabrication process and DTL exposure parameter.

The nanoring resist array was subsequently transferred into 600 nm SiN_x via dry etching using CHF_3 gas, followed by an oxygen plasma to remove the resist and BARC. Finally, the thick SiN_x nanoring array was used as an etch mask for the fabrication of axial InGaN/GaN nanotubes.

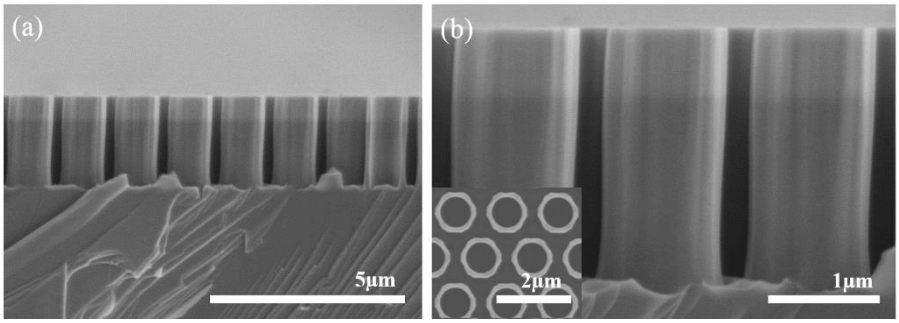

Fig. 2. (a) SEM cross-section image of the axial InGaN/GaN nanotube array obtained after the whole process for (a) low and (b) high magnification. The inset shows a SEM plan-view image of the axial InGaN/GaN nanotube array.

Optics EXPRESS

Figure 2 displays the obtained nanotubes after ICP Cl_2/Ar based chemistry etching performed at 250 °C and 9 mTorr. The nanotubes have an inner diameter of ~850 nm, a wall width of ~90-140 nm and a height of 2.42 µm. The dimensions and shape of the resist mask are perfectly transferred through the SiN_x mask into the InGaN/GaN LED template [inset in Figs. 2(b) and 3(a)] by carefully optimizing the etching parameters. In particular, the use of high temperature for GaN etching enables a reduction of the lateral roughness of the outer sidewall and leads to a slight undercut at the bottom part of the nanotube. Note, the cleaved nanotube on the far right of the SEM image in Fig. 2(a) where smooth inner sidewalls with a slight undercut are revealed. The SQW lies perpendicular to the longitudinal axis, in the upper lighter grey region of the nanotubes, above the slightly undercut section of the sidewalls. Note, the small reduction in sidewall thickness as a result of the undercut acts to decouple the SQW light emission from the GaN slab layer. The use of DTL enables the realization of an homogenous array of nanotubes across the whole 50 mm diameter wafer, with low size dispersion (~5%) when going from the center of the wafer to its edge. This fabrication technology can be easily scaled up to 100 mm on any wafers or LED structures.

3. Results and discussion

3.1 Hyperspectral cathodoluminescence

The optical emission of the axial InGaN/GaN nanotube array was assessed by room-temperature high-resolution cathodoluminsescence (CL) hyperspectral imaging [32]. The CL intensity image of a nanotube array, extracted between 350 nm and 650 nm, and displayed in Fig. 3(b), reveals higher emission intensity located at the axial position of the SQW for the whole array of InGaN/GaN nanotubes and on both their outer and inner surfaces.

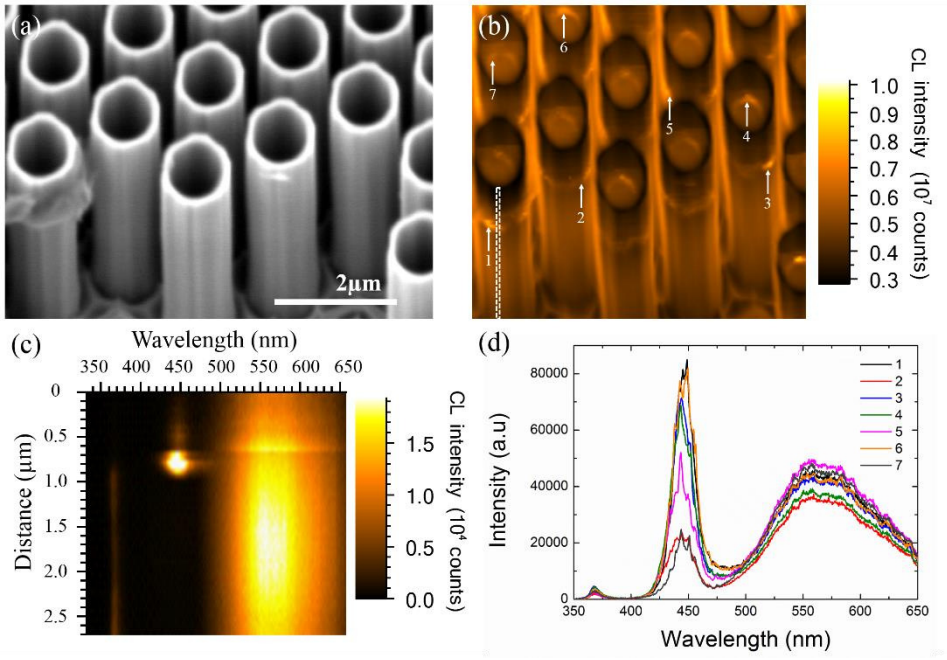

Fig. 3. (a) SEM image of the axial InGaN/GaN nanotube array. (b) CL intensity image extracted from the hyperspectral data over a 350-650 nm spectral range. The white dashed line on the bottom left hand side represents the position of the line scan presented in (c). The white arrow and related number are associated to the CL spectra display in (d). (c) Line scan CL spectra as a function of the position along the InGaN/GaN axial SQW nanotube outer facet. (d) CL spectra extracted from the hyperspectral data set at SQW positions for various InGaN/GaN nanotubes.

Optics EXPRESS

Figure 3(c) shows a spectral line scan extracted along the length of an individual InGaN/GaN nanotube [white dashed line in Fig. 3(b)] with the zero nm position corresponding to the top of the nanotube. As previously observed, the intense SQW peak occurs at ~444 nm and dominates the line scan. The GaN near-band-edge (NBE) emission around 367.5 nm is only observed in the n-type part (below the SQW). The yellow-band (YB) emission around 565 nm is observed along the whole nanotube length and originates from the defect-related YB emission of the initial template. CL spectra of the InGaN SQW emission extracted for various nanotubes are presented in Fig. 3(d). The InGaN/YB intensity ratio varies as a function of the nanotube and the position where the CL spectra is extracted, which could be related to variations in etch damage and/or light extraction/collection. The most interesting feature is the presence of well-defined resonances that modulate the 420-480 nm spectral range of the SQW emission.

3.2 Photoluminescence

To further investigate the optical properties and quality of the axial InGaN/GaN nanotubes, the nanostructures were mechanically removed from the substrate in an ultrasonic bath and then dispersed on a host sapphire substrate [Fig. 4(a)] to remove any contributions coming from the neighboring nanotubes or from the GaN slab layer. Although the quality of the bottom cleaved facet could impact the vertical FP mode quality, the SEM picture in Fig. 4(a) presents a nanotube with a reasonably good cleave. Continuous-wave (CW), 375-nm-excitation, power-dependent μPL [Figs. 4(b)-4(e)] and confocal PL experiments [Fig. 4(f)] were performed on such nanotube. Further details on the employed PL techniques can be found in the Experimental details section.

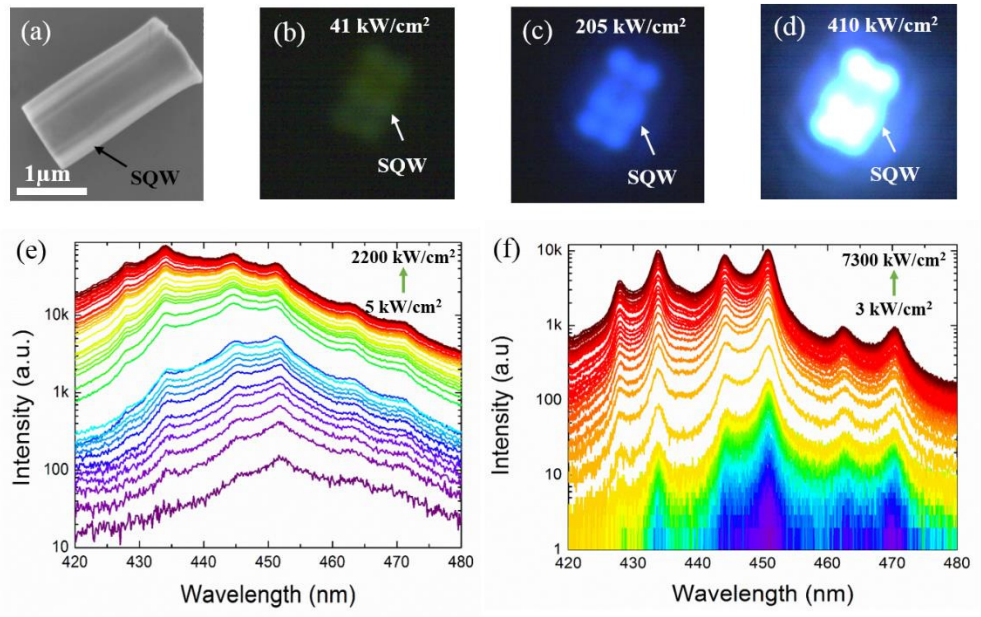

Fig. 4. (a) SEM images of a single dispersed InGaN/GaN nanotube. CCD images of a single InGaN/GaN nanotube pumped with μPL at (b) 41 kW/cm^2, (c) 205 kW/cm^2 and (d) 410 kW/cm^2. InGaN/GaN nanotube spectra for a continuous CW 375 nm excitation at RT with (e) μPL and (f) confocal microscope technique.

A change in the spectral distribution of the emission from a felled InGaN/GaN nanotube [Fig. 4(e)] can be observed when increasing the optical power. For a low excitation power density of 41 kW/cm^2, the emission across the nanotube length is almost uniform [Fig. 4(b)]. With the increase in power density to 205 kW/cm^2, the emission intensity starts to become

Optics EXPRESS

stronger on both ends of the nanotube and at the SQW position, which is then clearly enhanced for 410 kW/cm^2. The observed intensity distribution implies that the nanotubes not only supports vertical FPMs between the top and bottom facets, but also potentially WGMs localized at the SQW position. This result contrasts with earlier reports of bare GaN nanotubes in which only dominant FPM behavior was observed [22]. In general, given the geometry and refractive index steps of a nanotube structure, hybrid FP/WG modes are expected where the strength of the FP character is determined by the height of the nanotube and the location of the SQW relative to the end facets determining its length. Emission µPL spectra for excitation power density ranging from 5 kW/cm^2 to 2200 kW/cm^2 are displayed in Fig. 4(e), and confocal PL spectra for an excitation power density varying from 3 kW/cm^2 to 7300 kW/cm^2 in Fig. 4(f). Irrespective of the PL technique, several resonances centered at the same wavelengths appear in the observed spectrum. A non-linear increase of the intensity as evidence of lasing cannot be unambiguously extracted for any of the resonant mode. Moreover, it is observed in both experiments that the intensity of some of the resonances only gradually changes as a function of the excitation power density. For example, at low power excitation, the resonant peak at ~451 nm dominates the spectra, but with increasing excitation power density the intensity ratio between the 451 nm peak and the others significantly reduces.

Lasing action is generally more favorable when a high-quality confinement active region is used, such as multiple quantum well or quantum dot heterostructures [33–35], and if the emissive region couples strongly with one or more cavity modes of the structure.

3.3 Finite-difference time-domain simulations

FDTD simulations have been performed and compared with experiments to investigate the nature of the resonant modes, and the impact of the non-circular shape of the nanotube on the quality factors of the cavity and non-lasing action. A high magnification plan-view SEM picture of the nanotube has been used for simulation to take into account the non-circular shape of the outer diameter apparent in Fig. 3(a).

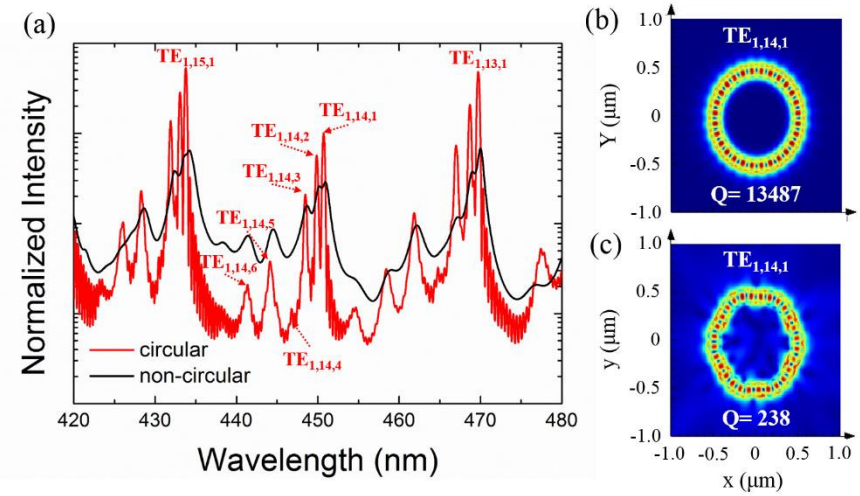

Fig. 5. (a) Normalized E-field intensity of a 2.4 µm tall InGaN/GaN nanotube with a circular and non-circular shape. Plan-view of the E-field magnitude snapshot of the ~451 nm resonant mode for (b) a circular and (c) non-circular geometry.

A single dipole source was placed at 600 nm from the top of a 2.42 µm high nanotube, i.e. at the SQW active region position. The spectrum of the dipole source had a Gaussian shape and the center wavelength and full width at half maximum of the spectrum was assumed to be

Optics EXPRESS

517 nm and 190 nm, respectively. The dipole source was polarized in the direction parallel to the SQW plane (i.e., electric field polarized along the c-plane) and thus excited the TE modes of the nanotube. Once the dipole source was generated inside the nanotube, the decay slope of the electromagnetic fields with respect to time was used to determine the resonant wavelengths and their associated Q-factors. Figure 5(a) displays the normalized E-field intensity obtained for a circular (in red) and non-circular (in black) nanotube for the wavelength range of the SQW emission (i.e., between 420 nm and 480 nm). The use of an intensity log scale allows clear extraction of all the resonances expected for such cavity structures. The non-circular outer diameter of the fabricated nanotube clearly impacts the resonant mode properties, leading to a decrease of the intensity, an increase in the full width at half maximum, a shift in their wavelength position and a merging of modes. This behavior can be explained by the break in symmetry between the inner and outer diameters which changes the light path within the cavity, thus impacting the quality of the cavity. As presented in the plan-view of the E-field magnitude snapshot in Figs. 5(b) and 5(c), for the resonant mode at ~451nm, less light is confined within the cavity and more light scattered inside and outside of the nanotube wall width, resulting in a lower confinement and thus in a decrease of the quality factor. These results suggest that the inner and outer geometry of the nanotube are an essential parameters to control in order to minimize optical losses and achieve stimulated emission.

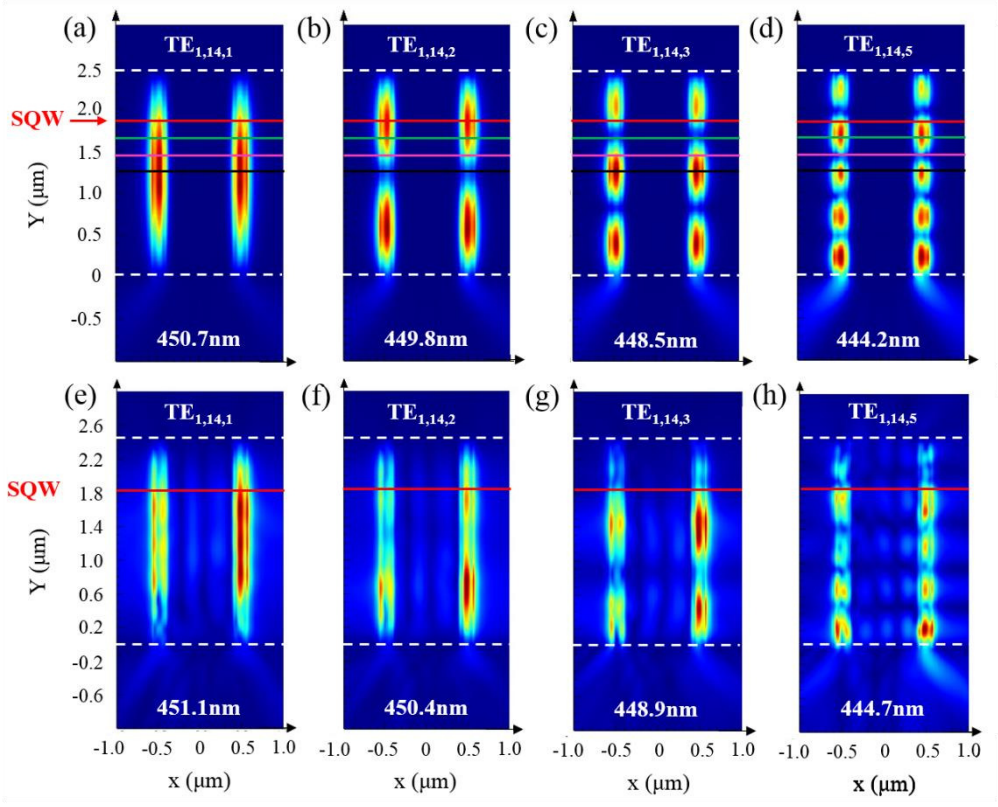

Fig. 6. Cross-section of the E-field magnitude snapshot of the 1st, 2nd, 3rd and 5th vertical orders of resonant FPMs component for (a-d) circular geometry and (e-h) non-circular geometry. The white dashed line delimit the bottom and top facets of the nanotube. The red line indicates the dipole/SQW position at 1820 nm. The green, purple and black lines are linked to the spectra in Fig. 8(b) and represent a gradual shift toward the middle of the nanotube with a 200 nm step.

Optics EXPRESS

Irrespective of the shape of the nanotube, nodes are still observed within the wall width of the nanotube [Figs. 5(b) and 5(c)], supporting the formation of resonances with a strong, possibly dominant WG character in the fabricated InGaN/GaN nanotube structures. The hybrid transverse electric WG/FP modes is characterized by $TE_{r,m,z}$ with r the radial mode order, m the angular mode order (i.e. node number/2) and z the vertical mode order (i.e. antinode number). The most intense resonant peaks observed at ~434 nm, ~451 nm and ~470 nm in Fig. 5(a) respectively are ascribed to the angular mode order number 15, 14 and 13 having a fundamental radial and vertical mode order component, as highlighted in Figs. 5(b) and 6(a) for the peak at ~451 nm. The series of peaks observed between each angular mode number are ascribed to an increase of the vertical mode order FP component of the cavity for a fixed WG radial and angular mode order. As demonstrated in Fig. 6, the cross-sections of the E-field magnitude extracted along the 2.42-µm-height circular nanotube successively shows an increase in the antinode number when going from ~451 nm to lower wavelength. Additionally, the intensity of the antinode along with the Q-factor is found to be lower when going to higher-order vertical modes. Plan view E-field magnitude snapshots produced by FDTD simulations show that no higher-order radial modes are predicted for the wall width considered. Similar observations are made in the cross-section E-field magnitude snapshot, where the non-circularity leads to a lower intensity of the antinode along with a lower Q-factor of the vertical mode. Additionally, the change in wall width and related non-circularity induce a variation of the antinode intensity across the circumference of the nanotube [between the left hand side and right hand side in Figs. 6(e)-6(h)] and a change in the number of antinodes [between Figs. 6(c) and 6(g)].

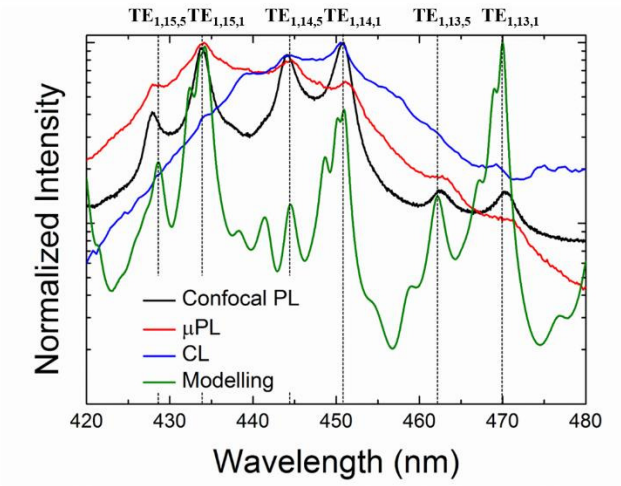

Fig. 7. Comparison between the normalized simulated field intensity and the normalized spectra for the employed CL/PL techniques.

Comparing experimental data with FDTD simulation, as presented in Fig. 7, enables the nature of the resonances observed in CL, µPL and confocal PL to be identified. A clear pattern of two resonances spaced by ~7 nm can be observed in CL/PL techniques and unambiguously ascribed to a hybrid cavity resonance having a mixed WGM character combined with a family of vertical Fabry-Perot modes (i.e. the fundamental FP vertical mode order and the 5th FP higher-order vertical mode). Further comparison shows that the FWHMs of the resonance emission peaks observed by CL/PL are much broader than those obtained by FDTD simulation, suggesting that experimental peaks at ~434 nm, ~451 nm and ~470 could actually be a convolution of the fundamental and second FP vertical mode order. The observation of the 5th higher-order vertical FPM in CL/PL spectra rather than another higher-order vertical mode can be explained by the position of the active region along the length of

Optics EXPRESS

the nanotube [as depicted by the red lines in Fig. 6]. Since the SQW was 600 nm below the top of the 2.42 µm height nanotube, one would expect that antinodes from FP higher-order vertical mode placed around 1.82 µm will efficiently couple with the active region, as it the case for the first, the second and the fifth order [Fig. 6(e), 6(f) and 6(h)], and leads to an enhancement of these modes. Thus, the coupling of light into higher-order modes can be enhanced or suppressed by varying the height of the nanotube and/or by varying the position of the active region during epitaxial growth.

In order to validate our assumption and investigate the potential route to follow to reduce the number of modes contributing to the emission, additional simulations were performed for circular nanotubes as a function of the height and the position of the active region. Figure 8(a) shows the impact of changing the height of the nanotube with the SQW placed 600 nm below the top. Fewer higher order vertical FP modes contribute when the height of the nanotube is decreased, with only two ($TE_{1,14,2}$, $TE_{1,14,3}$) and one ($TE_{1,14,2}$) higher-order mode, for a height of 1620 nm and 720 nm, respectively, against six modes for a height of 2420 nm. However, the reduction of modes contributing to the emission is achieved at the cost of a reduction of the Q-factor.

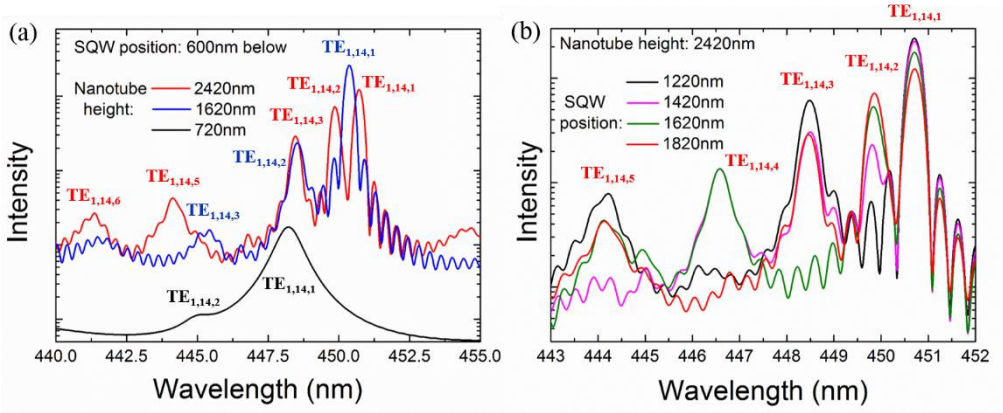

Fig. 8. (a) E-field intensity of a 2.4 µm, 1.6 and 700 nm tall InGaN/GaN nanotube with a SQW 600nm bellow. (b) E-field intensity of a 2.4 µm tall InGaN/GaN nanotube with a SQW changing from the center of the nanotube at 1220 nm to the actual experimental position of the SQW at 1820 nm.

Figure 8(b) shows the impact of changing the position of the active region (the dipole vertical position) for a fixed nanotube height of 2420 nm. Each position plotted in Fig. 8(b) is shown in Figs. 6(a)-6(c) and d with the same color code. At the middle of the nanotube (1220 nm) the SQW preferentially couples with the odd vertical FP modes. This is clearly seen in the black curve in Fig. 8(b). As the SQW moves away from the center the intensity of $TE_{1,14,1}$ will decrease. For higher-order vertical modes the position of the SQW can couple to other antinodes. For example, the intensity of $TE_{1,14,2}$ will become a maximum for a SQW positioned at 1820 nm [red curve in Fig. 8(b)]. The same trend can be observed for the higher order vertical modes.

Therefore, one route to achieve a reduction in the number of modes contributing to lasing while maintaining good coupling with the fundamental FP vertical mode is to position the active region slightly above the middle of the nanotube (e.g. at around 1420 nm for these nanotubes of height 2420 nm) where it still couples efficiently with the fundamental mode and weakly with the second, third, fourth and fifth order [pink curve in Fig. 8(b)].

4. Conclusion

In summary, a low-cost fast and large scale fabrication process for tube cavities has been reported by a combination of Displacement Talbot lithography and inductively coupled

Optics EXPRESS

plasma (ICP) top-down etching. The flexibility of the patterning process, by tuning the pattern configuration of the amplitude mask, allows the design of tube arrays with a broad range of diameter and pitch. This process can be transferred on any type of wafer, with no impact of the template surface roughness on the patterning process.

The optical emission and modal properties of axial InGaN/GaN nanotubes created from a SQW LED structure revealed homogeneous emission from nanotube to nanotube along with vertical light confinement between the bottom and top facets and radial confinement within the active region. Correlation with FDTD simulation suggests that both mixed WG – FP cavity modes are observed within the single nanotube. Simulations further demonstrate that the inner and outer geometry of the nanotube is an essential parameter to control in order to minimize optical losses. By combining a high-quality confinement active region, a perfect circular symmetry and an optimum height and positioning of the active region around the middle height of the nanotube, the WG modal properties are predicted to be enhanced. Furthermore, lasing emission with a reduced number of modes overlapping with the active region emission should be achieved. These results not only open new perspectives for the fabrication of electrically injected WG-based lasers in the whole UV-Visible-IR wavelength range, but also for bio-chemical sensing applications.

5. Experimental details

5.1 DTL exposure and resist development

The gap between the mask and the wafer was set to 150 µm. The range of displacement was set to two Talbot lengths, i.e. 17.6 µm. A coherent 375 nm illumination source with an energy density of 1 $mW.cm^{-2}$ was used. Real time control of the energy density of the source allow an accurate exposure dose. After exposure, the sample was baked for 1 min 30 sec at 120°C on a hot plate. The sample was developed in MF-CD-26 developer for 30 sec, rinsed with deionized water and dried with nitrogen.

5.2 ICP top-down dry etching

The etching was performed in an inductively coupled plasma (ICP) dry etch system (Oxford Instruments System 100 Cobra) using the following recipe: 1) for SiN_x ring etching a CHF_3 flow of 25 sccm, 50 W RF power, 300 W ICP source power, 8 mTorr and 20°C for 12 min; 2) for GaN nanotube etching a Cl_2 flow of 50 sccm, an Ar flow of 10 sccm, 120 W RIE power, 800 W ICP source power, 9 mTorr and 250°C for 330 sec.

5.3 CL characterization

Cathodoluminescence hyperspectral imaging measurements were carried out at room temperature in a modified FEI Quanta 250 field emission SEM using electron energies of 5.0 keV and beam currents of approximately 1 nA. Light was collected using an NA 0.28 reflecting objective with its axis perpendicular to the electron beam and focused directly on the entrance of the spectrograph using an off-axis paraboloidal mirror. We used a 125 mm focal length spectrograph with a 600 lines/mm grating and 50 µm entrance slit, coupled to a cooled electron multiplying charge-coupled device (EMCCD) detector.

5.4 µPL characterization

µPL characterization was carried out on single nanotube cavities in an in-house made micro-PL system. A 375 nm continuous wave (CW) laser diode was used to selectively excite the InGaN/GaN SQW. A 50x magnification, 0.43 NA objective was used to focus the excitation laser down to ~2µm and collect the emission through a 1 mm fibre bundle. A 0.55 m Jobin Yvon spectrometer (iHR550) was used to disperse the emission and the emission was detected with an air-cooled charge coupled device (CCD). The system was equipped with X-

Optics EXPRESS

Y-Z motorized stages allowing to selectively excite single nanotubes. All the measurements were performed at room temperature.

5.5 Confocal PL characterization

Confocal PL characterization was performed using a commercial WITec confocal microscope. A 375 nm continuous wave (CW) diode laser was used as an optical pumping source and the system was equipped with a 300 mm Princeton instruments monochromator (SP2300i) and an air-cooled charge coupled device (CCD). An objective lens (100 × , NA = 0.95) was used to focus the laser beam down to a spot with a diameter of ~400 nm. The emission was dispersed by the monochromator with a resolution of ~0.1 nm. An optical fiber with a diameter of 10 µm acted as a pinhole, thus allowing the emission to be collected from only where the sample was excited. The system was equipped with a high-resolution x-y-z piezo-stage to individually address and examine single nanotubes. The spatial resolution of the system was ~160 nm. All the measurements were performed at room temperature.

5.6 FDTD simulation

A three-dimensional finite difference time domain (FDTD) approach has been used to simulate the nanotube structure using commercial-grade software [Lumerical Solutions, Inc. http://www.lumerical.com/tcad-products/fdtd/]. A dipole source with emission wavelengths from 370 to 720 nm was vertically positioned in the plane of the nanotube quantum wells and centred within the width of the walls. All the geometrical data used for the simulation are from the SEM measurement of our nanotube. The n-GaN, p-GaN and GaN-substrate layers are given a refractive index defined by ellipsometry measurements performed on the as-grown structure at the University of Strathclyde. The InGaN quantum well layer is 3nm thick (n = 2.6). There is a minimum of fifteen mesh cells per wavelength in the simulation that is run for 2000fs. Frequency-domain power monitors have been used to record the emission profile over the simulation region, which is surrounded by perfectly matched layer absorbing boundaries on all sides. The simulated spectra are collected by a grid of 12 time-monitors placed at various points inside the nanotube structure, accurately calculating the envelope of the time-domain field signal. For the perfectly-circular higher-Q examples, each resonant peak is isolated in the frequency domain using a Gaussian filter, and by taking the inverse Fourier transforms the time decay have been calculated separately for each peak. The slope of the time decay is used to calculate the Q-factor of each resonance. In the DTL fabricated structures, the electromagnetic fields decay completely from the simulation in a time that can be simulated reasonably by FDTD. Therefore, the resonant frequencies are found from the time-monitors along with the full-width half-maximum (FWHM) of the corresponding peaks. We can then use $Q = f_R/\Delta f$ where f_R is the resonant frequency and Δf is the FWHM.

Funding

Engineering and Physical Sciences Research Council (EPSRC), UK, Grant No. EP/M015181/1, “Manufacturing nano-GaN”.

Acknowledgments

The authors would like to thank OSRAM for the provision of the InGaN/GaN LEDs templates.

Data sets

This publication is supported by multiple data sets, which are openly available here: https://doi.org/10.15125/BATH-00414